Thermal Radiation and Magnetic Effects on Coupled Heat and Mass Transfer by Mixed Convection about a Wedge in Porous Media: The Entire Regime

熱輻射與磁場效應對於流經飽和多孔性介質內一楔形面混合對流之熱傳與質傳 的影響:整個範圍

> Kuo-Ann Yih 易 國 安

Department of Aircraft Engineering, Air Force Institute of Technology 飛機工程系,空軍航空技術學院

Abstract

The thermal radiation and magnetic effects on coupled heat and mass transfer by mixed convection flow about a wedge in porous media are numerically analyzed. The surface of the wedge is maintained at uniform wall temperature and uniform wall concentration (UWT/UWC). Rosseland diffusion approximation is adopted for the radiative heat flux. The transformed governing equations are solved by Keller box method (KBM). Comparisons with previously published work are performed and the results are found to be in good agreement. Numerical results for the dimensionless temperature profile, the dimensionless concentration profile, the local Nusselt number and the local Sherwood number are displayed graphically and tabularly to illustrate the influence of the buoyancy ratio N, the Lewis number Le, the wedge angle parameter m, the magnetic parameter M, the mixed convection parameter χ , the radiation-conduction parameter χ , and the surface temperature parameter H. The entire regime of the mixed convection is included, when χ varies from 0 (pure free convection) to 1 (pure forced convection). The physical aspects of the problem are discussed in details.

Keywords: thermal radiation and magnetic effects, heat and mass transfer, mixed convection, wedge, porous media

摘要

本文以一數值方法來分析:熱輻射與磁場效應對於流經飽和多孔性介質內一楔形面混合對流之熱傳與質傳的影響。楔形面的表面維持於均勻壁溫度與均勻壁濃度之條件。輻射熱通量係採用羅斯蘭特擴散近似法。吾人以凱勒盒子法來解轉換過的控制方程式。所得的數值計算結果與已刊登發表的期刊論文結果作比較,結果非常吻合。所得到的數值計算結果主要以

圖形與表格來顯示:浮力比,路易士數,楔形角度參數,磁性參數,混合對流參數,輻射—傳導參數,與表面溫度參數,對於無因次溫度分佈、無因次濃度分佈、局部紐塞爾數和局部希爾吾德數之影響。當混合對流參數從 0(純自然對流)變化到 1(純強制對流)時,則包括了混合對流的整個範圍。文中的物理現象也詳加討論。

關鍵字:熱輻射與磁場效應,熱傳與質傳,混合對流,楔形面,多孔性介質

1. Introduction

Coupled heat and mass transfer (or double-diffusion) driven by buoyancy, due to temperature and concentration variations in a saturated porous medium, has several important applications in geothermal and geophysical engineering, for example, the migration of moisture in fibrous insulation and the underground disposal of nuclear wastes. Recent book by Nield and Bejan [1] presents a comprehensive account of the available information in the field.

In the aspect of pure heat transfer by mixed convection, Cheng [2] studied combined free and forced convection flow about inclined surfaces in porous media. Lai and Kulacki [3] extended the work of Cheng [2] to investigate the influence of lateral mass flux on mixed convection over inclined surfaces in saturated porous media. Nonsimilar solution for mixed convection on a wedge embedded in a porous medium was examined by Vargas et al. [4]. Kumari and Gorla [5] introduced a single parameter (the mixed convection parameter) for the entire regime of free-forced-mixed convection and analyzed combined convection along a variable non-isothermal wedge with wall temperature (VWT) in a porous medium.

In the aspect of coupled heat and mass transfer by mixed convection, Yih [6] spread the research of Kumari and Gorla [5] to present coupled heat and mass transfer in mixed convection over a wedge with variable wall temperature and concentration (VWT/VWC) in porous media: the entire regime. Yih [7] examined the uniform transpiration effect on coupled heat and mass transfer in mixed convection about inclined surfaces (VWT/VWC) in porous media: the entire regime, which is the extension study of Lai and Kulacki [3]. Cheng [8] followed the step of Yih [6] to study Soret and Dufour effects on mixed convection heat and mass transfer from a vertical wedge in a porous medium with constant wall temperature and concentration (UWT/UWC).

There has been renewed interest in studying magnetohydrodynamic (MHD) flow and heat transfer in porous media due to the effect of magnetic fields on flow control and on the performance of many systems using electrically-conducting fluids. Chamkha and Khaled [9] investigated the nonsimilar hydromagnetic simultaneous heat and mass transfer by mixed convection from a vertical plate embedded in a uniform porous medium. Cheng [10] studied an integral approach for hydromagnetic natural convection heat and mass transfer from vertical surfaces with power-law variation in temperature and concentration (VWT/VWC) in porous media. Very recently, Cheng [11] extended the special cases of Yih [6] and Cheng [10] to analyze effect of a magnetic field on mixed convection heat and mass transfer from a vertical wedge subjected to uniform wall temperature and uniform wall concentration (UWT/UWC) in a porous medium utilizing an integral approach.

As the difference between the surface temperature and the ambient temperature is large, it may cause the thermal radiation effect to become important. Hossain and Takhar [12] used the Rosseland diffusion approximation and maintained the T⁴ term to study radiation effect on mixed convection along a vertical plate with uniform wall temperature (UWT). Yih [13] extended the special case of Kumari and Gorla [5] to investigate radiation effect on mixed convection over an isothermal wedge in porous media: the entire regime. Radiation and blowing/suction effects on mixed convection over an isothermal vertical cylinder in porous media for the entire regime was studied by Yih [14]. Chamkha et al. [15] spread the work of Yih [13] to examine the radiation effects on mixed convection over an isothermal wedge embedded in a porous medium filled with a nanofluid.

The objective of the present work, therefore, is to extend the work of Cheng [11] and Yih [13] to investigate numerically the magnetic and thermal radiation effects on coupled heat and mass transfer by mixed convection about a wedge subjected to uniform wall temperature and uniform wall concentration (UWT/UWC) in porous media: the entire regime. The governing equations have been solved numerically using Keller box method (KBM). The results are obtained for various values of the parameters.

2. Analysis

Considering the problem of combined heat and mass transfer by mixed convection flow over a wedge with half angle γ embedded in a saturated

porous medium with an optically dense, electrically conducting fluid in the presence of a transverse magnetic field for the entire regime. The surface of wedge is maintained at uniform wall temperature and uniform wall concentration (UWT/UWC). Figure 1 shows the flow model and physical coordinate system. The origin of the coordinate system is placed at the leading edge of the wedge, where x is the coordinate along the surface of wedge measured from the origin and y is the coordinate normal to the surface, respectively [13]. The uniform wall temperature T_w is greater than the ambient temperature T_{∞} . The flow over the wedge is assumed to be two-dimensional, laminar, steady and incompressible. Fluid properties are assumed to be constant except the density variations in the buoyancy force term.

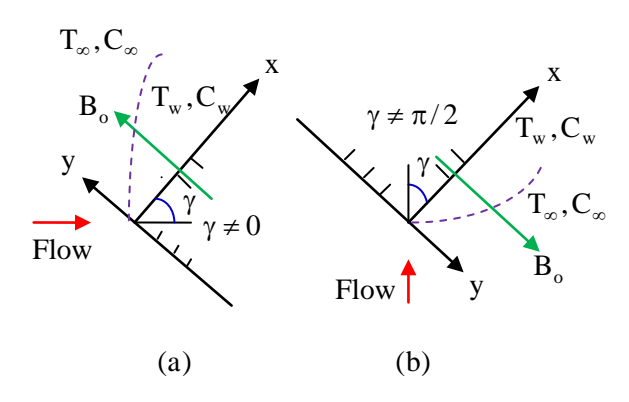


Fig. 1. Flow model and physical coordinate system

The applied transverse magnetic field is assumed to be uniform and the magnetic Reynolds number is so small that induced magnetic field can be neglected. Further, the external electric field is assumed to be zero and the electric field due to polarization of charges is negligible [11].

Introducing the boundary layer approximation, the Boussinesq approximation, and Rosseland

diffusion approximation, the governing equations based on the Darcy law (It is valid under the condition of low velocity and small pores of porous medium [16]) can be written as follows [11, 13]: Continuity equation:

$$\frac{\partial \mathbf{u}}{\partial \mathbf{x}} + \frac{\partial \mathbf{v}}{\partial \mathbf{y}} = \mathbf{0} \tag{1}$$

Momentum (Darcy) equation:

$$u + \frac{K\sigma B_0^2}{\mu} u = -\frac{K}{\mu} \left(\frac{\partial p}{\partial x} + \rho g \cos \gamma \right) \eqno(2)$$

$$v = -\frac{K}{\mu} \left(\frac{\partial p}{\partial y} + \rho g \sin \gamma \right)$$
 (3)

Energy equation:

$$u\frac{\partial T}{\partial x} + v\frac{\partial T}{\partial y} = \alpha \frac{\partial^2 T}{\partial y^2} - \frac{1}{\rho_{\alpha} C_{P}} \frac{\partial q_{r}}{\partial y}$$
(4)

Concentration equation:

$$u\frac{\partial C}{\partial x} + v\frac{\partial C}{\partial y} = D_M \frac{\partial^2 C}{\partial y^2}$$
 (5)

Boussinesq approximation:

$$\rho = \rho_{\infty} \left[1 - \beta_{T} \left(T - T_{\infty} \right) - \beta_{C} \left(C - C_{\infty} \right) \right] \tag{6}$$

Rosseland diffusion approximation:

$$q_{r} = -\frac{4\sigma_{0}}{3(a_{r} + \sigma_{s})} \frac{\partial T^{4}}{\partial y} = -\frac{16\sigma_{0}}{3(a_{r} + \sigma_{s})} T^{3} \frac{\partial T}{\partial y}$$
 (7)

Boundary conditions:

$$y = 0$$
: $v = 0$, $T = T_w$, $C = C_w$, (8)

$$y = 0$$
: $u = U_{\infty}$, $T = T_{\infty}$, $C = C_{\infty}$, (9)

Here, u and v are the components of the Darcy velocity in the x and y directions, respectively; g is the gravitational acceleration; K is the permeability of the porous medium; σ and B_o are the electrical conductivity of the fluid and the externally imposed magnetic field in the y-direction; $\mu,\,p$ and ρ are the viscosity, the pressure and the density of the fluid, respectively; T and C are the volume-averaged temperature and concentration, respectively; α and D_M are the equivalent thermal diffusivity and mass diffusivity, respectively; C_P is

the specific heat at constant pressure; q_r is the radiative heat flux; β_T and β_C are the thermal and concentration expansion coefficients of the fluid, respectively; σ_o , a_r , σ_s are the Stefan-Boltzmann constant, the Rosseland mean extinction coefficient, and the scattering coefficient, respectively. The term $16\sigma_0 T^3/[3(a_r + \sigma_s)]$ can be considered as the "radiative conductivity" [13].

The external flow is at a uniform temperature $T_{\infty} \text{ and uniform concentration } C_{\infty} \text{ with velocity}$

$$U_{\infty} = Bx^{m}, \quad m = \gamma/(\pi - \gamma)$$
 (10)

where B is a prescribed constant and m is the wedge angle parameter. Specifically, the cases of m = 0, 1/3 and 1 correspond, respectively, to a uniform free stream flowing along a vertical flat plate, a free stream flowing over a 90° wedge, and a stagnation flow normal to a vertical wall.

The stream function ψ is defined by

$$u = \partial \psi / \partial y$$
, $v = -\partial \psi / \partial x$. (11)

Therefore, the continuity equation is automatically satisfied.

Now paying attention to governing equations the operation of If we do cross-differentiation: $\partial(2)/\partial y - \partial(3)/\partial x$, then the pressure terms in equations (2)-(3) can be eliminated. Further, with the help of the equation (6), the boundary laver approximation $(\partial/\partial x << \partial/\partial y, \ v << u)$, $\cos \gamma$ and $\sin \gamma$ are of the same order of magnitude (the buoyancy force normal to the heated surface is negligible). The last approximation is valid for a wedge range of wedge angle except near $\gamma = 0^{\circ}$ in Figure 1(a) or near $\gamma =$ 90° in Figure 1(b) [13]. Then we can obtain

$$\left(1 + \frac{K\sigma B_0^2}{\mu}\right) \frac{\partial u}{\partial y} = \frac{\rho_\infty g \cos \gamma K}{\mu} \left(\beta_T \frac{\partial T}{\partial y} + \beta_C \frac{\partial C}{\partial y}\right)$$
(12)

Integrating equation (12) once and with

the aid of equation (9), then we get

$$\left(1 + \frac{K\sigma B_o^2}{\mu}\right) \left(u - U_{\infty}\right) = \frac{\rho_{\infty}g\cos\gamma K}{\mu} \left[\beta_T \left(T - T_{\infty}\right) + \beta_C \left(C - C_{\infty}\right)\right] \tag{13}$$

Inserting equation (4) into (7), the energy equation (4) becomes

$$u\frac{\partial T}{\partial x} + v\frac{\partial T}{\partial y} = \alpha \frac{\partial^2 T}{\partial y^2} + \frac{16\sigma}{3(a_r + \sigma_s)\rho_\infty C_p} \frac{\partial}{\partial y} \left(T^3 \frac{\partial T}{\partial y}\right). \tag{14}$$

Invoking the following dimensionless variables:

$$\chi = \left[1 + \left(\frac{Ra_x}{Pe_x} \right)^{1/2} \right]^{-1} = \frac{Pe_x^{\frac{1}{2}}}{Pe_x^{\frac{1}{2}} + Ra_x^{\frac{1}{2}}}$$
 (15.1)

$$\eta = \frac{y}{x} Pe_x^{\frac{1}{2}} \chi^{-1} = \frac{y}{x} \left(Pe_x^{\frac{1}{2}} + Ra_x^{\frac{1}{2}} \right)$$
 (15.2)

$$f(\chi, \eta) = \frac{\Psi}{\alpha Pe_{x}^{\frac{1}{2}} \chi^{-1}} = \frac{\Psi}{\alpha \left(Pe_{x}^{\frac{1}{2}} + Ra_{x}^{\frac{1}{2}}\right)}$$
(15.3)

$$\theta(\chi, \eta) = \frac{T - T_{\infty}}{T_{w} - T_{\infty}} \tag{15.4}$$

$$\phi(\chi, \eta) = \frac{C - C_{\infty}}{C_{w} - C_{\infty}}$$
 (15.5)

$$Pe_{x} = \frac{U_{\infty}x}{\alpha}$$
 (15.6)

$$Ra_{x} = \frac{\rho_{\infty}g\cos\gamma\beta_{T}(T_{w} - T_{\infty})Kx}{\mu\alpha} \qquad (15.7)$$

where Pe_x and Ra_x are the local Peclet number and the modified local Rayleigh number for the flow through the porous medium, respectively. χ is the mixed convection parameter. It is noted that $\chi=0$ ($Pe_x=0$) and $\chi=1$ ($Ra_x=0$) correspond to pure free and pure forced convection cases, respectively. The entire regime of mixed convection corresponds to the values of χ between 0 and 1.

Substituting equation (15) into equations

(13)-(14), (5), (8)-(9), then we can achieve

$$(1+M^2) f' = (1-\chi)^2 (\theta + N\phi) + (1+M^2) \chi^2,$$
(16)

$$\begin{split} \theta'' + \frac{1 + m\chi}{2} f \theta' + \frac{4R_d}{3} \left\{ & \theta' [(H - 1)\theta + 1]^3 \right\}' \\ & = \frac{m}{2} \chi (1 - \chi) \left(f' \frac{\partial \theta}{\partial \chi} - \theta' \frac{\partial f}{\partial \chi} \right), \end{split} \tag{17}$$

$$\frac{1}{\text{Le}}\phi'' + \frac{1+m\chi}{2}f\phi' = \frac{m}{2}\chi(1-\chi)\left(f'\frac{\partial\phi}{\partial\chi} - \phi'\frac{\partial f}{\partial\chi}\right). \tag{18}$$

The boundary conditions are defined as follows:

$$\eta = 0$$
: $f = 0$, $\theta = 1$, $\phi = 1$, (19)

$$\eta \to \infty$$
: $\theta = 0$, $\phi = 0$. (20)

In the above equations, the primes denote the differentiation with respect to η . Besides, the magnetic parameter M, the buoyancy ratio N, the Lewis number Le, the radiation-conduction parameter R_d , and the surface temperature parameter H, are defined as followed, respectively:

$$M = \sqrt{\frac{K\sigma B_o^2}{\mu}}$$
 (21)

$$N = \frac{\beta_{\rm C}(C_{\rm w} - C_{\infty})}{\beta_{\rm T}(T_{\rm w} - T_{\infty})}, \qquad \text{Le} = \frac{\alpha}{D_{\rm M}}$$
 (22)

$$R_{d} = \frac{4\sigma_{0}T_{\infty}^{3}}{k(a_{r} + \sigma_{s})}, \qquad H = \frac{T_{w}}{T_{\infty}}$$
 (23)

In addition, the Darcian velocity components are

$$u = U_{\infty} \chi^{-2} f' = \frac{\alpha}{x} \left(P e_{x}^{\frac{1}{2}} + R a_{x}^{\frac{1}{2}} \right)^{2} f', \qquad (24)$$

$$\begin{split} v &= -\frac{\alpha P e_x^{\frac{1}{2}}}{x} \chi^{-1} \bigg\{ \frac{1}{2} \big[1 + m \chi \big] f \\ &- \frac{1}{2} \big[1 - m \chi \big] \eta f' + \frac{m}{2} \chi (1 - \chi) \frac{\partial f}{\partial \chi} \bigg\}. \end{split} \tag{25}$$

The results of practical interest in many applications are both the surface heat and mass transfer rates. The surface heat and mass transfer

rates are expressed in terms of the local Nusselt number Nu_x and the local Sherwood number Sh_x respectively, which are basically defined as followed:

$$Nu_{x} = \frac{h_{x}x}{k} = \frac{q_{w}x}{(T_{w} - T_{w}) k}.$$
 (26)

$$Sh_{x} = \frac{h_{m,x}x}{D_{M}} = \frac{m_{w}x}{(C_{w} - C_{\infty}) D_{M}}.$$
 (27)

where h_x , $h_{m,x}$ are local convective heat transfer coefficient and local convective mass transfer coefficient, respectively; k is the equivalent thermal conductivity; q_w and m_w are the local heat flux and the local mass flux, respectively; and $q_w = h_x \left(T_w - T_\infty \right)$ (the Newton's law of cooling) and $m_w = h_{m,x} \left(C_w - C_\infty \right)$ (the analogy between the mass transfer and the heat transfer).

From the Fourier's law of heat conduction, the Rosseland diffusion approximation and the Fick's law of mass diffusion, the rate of surface heat transfer q_w and the rate of surface mass transfer m_w are defined as followed, respectively:

$$\begin{split} \boldsymbol{q}_{\mathrm{w}} &= \boldsymbol{q}_{\mathrm{cond}} + \boldsymbol{q}_{\mathrm{r}} = -k \Bigg(\frac{\partial T}{\partial \boldsymbol{y}} \Bigg) \Bigg|_{\boldsymbol{y} = \boldsymbol{0}} - \frac{16 \sigma_{0} T^{3}}{3 \big(\boldsymbol{a}_{\mathrm{r}} + \boldsymbol{\sigma}_{s}\big)} \Bigg(\frac{\partial T}{\partial \boldsymbol{y}} \Bigg) \Bigg|_{\boldsymbol{y} = \boldsymbol{0}} \\ &= - \Bigg\{ \Bigg[k + \frac{16 \sigma_{0} T^{3}}{3 \big(\boldsymbol{a}_{\mathrm{r}} + \boldsymbol{\sigma}_{s}\big)} \Bigg] \Bigg\} \Bigg(\frac{\partial T}{\partial \boldsymbol{y}} \Bigg) \Bigg|_{\boldsymbol{y} = \boldsymbol{0}}. \end{split}$$

 $m_{\rm w} = -D_{\rm M} \left(\frac{\partial C}{\partial y} \right)$ (29)

Inserting equations (28)-(29) into equations (26)-(27) and with the aid of equation (15), the local Nusselt number Nu_x and the local Sherwood number Sh_x in terms of $Pe_x^{1/2} + Ra_x^{1/2}$ are, respectively, obtained by

$$\frac{Nu_x}{Pe_x^{1/2} + Ra_x^{1/2}} = \left(1 + \frac{4R_dH^3}{3}\right) \left[-\theta'(\chi,0)\right] \quad (30)$$

$$\frac{Sh_{x}}{Pe_{x}^{\frac{1}{2}} + Ra_{x}^{\frac{1}{2}}} = \left[-\phi'(\chi, 0) \right]$$
 (31)

When $\chi = 1$ (pure forced convection) and $R_d = 0$ (in the absence of radiation), equations (16)-(18) can be reduced to

$$f' = 1, (32)$$

$$\theta'' + \frac{1+m}{2}f\theta' = 0, (33)$$

$$\phi'' + \frac{(1+m)Le}{2}f\phi' = 0.$$
 (34)

Solving the above equations (32)-(34) and the boundary conditions (19)-(20), by separation of variables, we can find

$$-\theta'(1,0) = \sqrt{\frac{1+m}{\pi}}, -\phi'(1,0) = \sqrt{\frac{(1+m)Le}{\pi}}.$$
 (35)

It may be noticed that for $R_d=0$, equations (16)-(20) are reduced to those of Cheng [11]. For the case of N=0 (pure heat transfer) and M=0 (in the absence of magnetic field), equations (16)-(17), (19.1-2)-(20.1) are reduced to those of Yih [13] (The boundary value problem for ϕ then becomes ill-posed and is of no physical significance). It is also observed that similar equations are obtained for the case of $\chi=0$ or $\chi=1$ or m=0.

3. Numerical Method

The present analysis integrates the system of equations (16)-(20) by the implicit finite difference approximation together with the modified Keller box method of Cebeci and Bradshaw [17]. To begin with, the differential equations are first converted into a system of five first-order equations. Then these first-order equations are expressed in finite difference forms and solved along with their boundary conditions by an iterative scheme. This approach gives a better rate of convergence and

(28)

reduces the numerical computational times.

Computations were carried out on a personal computer with the first step size $\Delta\eta_1=0.01$. The variable grid parameter is chosen 1.01 and the value of $\eta_\infty=100$. The iterative procedure is stopped to give the final temperature and concentration distributions when the errors in computing the θ_w' and ϕ_w' in the next procedure become less than 10^{-5} .

4. Results and Discussion

In order to verify the accuracy of our present method, we have compared our results with those of Yih [6, 13, 20-21], Cheng [11, 19], Bejan and Khair [18], and Chamkha et al. [15]. Table 1 lists the comparison of the values of $-\theta'(1,0)$ for various values of m with M = 0, $R_d = 0$. Table 2 shows the comparison of the values of $-\phi'(1,0)$ for various values of m and (a) Le = 0.01, (b) Le =1, (c) Le = 100 with M = 0, $R_d = 0$. Table 3 shows the comparison of the values of $-\theta'(\chi,0)$ for various values of with N = 0, m = 1/3, M = 0, $R_d =$ 0. Tables 4 and 5 list the comparison of the values of $-\theta'(0,0)$ and $-\phi'(0,0)$ for various values of N and Le with m = 0, M = 0, $R_d = 0$, respectively. Table 6 depicts the comparison of the values of $-\theta'(\chi,0)$ and $-\phi'(\chi,0)$ for various values of Le with N = 1, m = 1/2, M = 0, $R_d = 0$, respectively. Table 7 lists the comparison of the values of $Nu_{_{X}}\,/(Pe_{_{X}}^{\frac{1}{2}}+Ra_{_{X}}^{\frac{1}{2}})\,$ for various values of R_{d} and Hwith N = 0, M = 0, $\chi = 0$. Table 8 reveals the comparison of the values of $Nu_x/(Pe_x^{\frac{1}{2}} + Ra_x^{\frac{1}{2}})$ for various values of χ , R_d and m with N = 0, M = 0, H = 1.0001. The comparisons in all the above cases are almost found to be in excellent agreement, as shown in Tables 1-8.

However, the results of Cheng [11] (integral method) in Table 3 are under-estimated for χ approaches to 0, while over-estimated for χ approaches to 1. The results of Cheng [19] (integral method) in Tables 4 and 5 are over-predicted for all values of N and Le.

Table 1 Comparison of the values of $-\theta'(1,0)$ for various values of m with M = 0, $R_d = 0$

	$-\theta'(1,0)$						
m	Yih	Chamkha et					
	[13]	al. [15]	Eq. (35)	results			
0	0.5642	0.5642	0.5642	0.5642			
1/4			0.6308	0.6308			
1/3	0.6515	0.6516	0.6515	0.6515			
1/2			0.6910	0.6910			
3/4		_	0.7463	0.7463			
1	0.7979	0.7979	0.7979	0.7979			

Table 2 Comparison of the values of $-\phi'(1,0)$ for various values of m and (a) Le = 0.01,

(b) Le = 1, (c) Le = 100 with M = 0, $R_d = 0$

	, , ,		<u> </u>
(0)		$-\phi'(1,0)$	
(a)	V:1, [6]	E~ (25)	Present
Le = 0.01	Yih [6]	Eq. (35)	results
m = 0	0.0564	0.0564	0.0564
m = 1	0.0798	0.0798	0.0798
(b)	Yih [6]	E = (25)	Present
Le = 1	1111 [0]	Eq. (35)	results
m = 0	0.5642	0.5642	0.5642
m = 1	0.7979	0.7979	0.7979
(c)	V:h [6]	Eq. (25)	Present
Le = 100	Yih [6]	Eq. (35)	results
m = 0	5.6418	5.6419	5.6417
m = 1	7.9789	7.9788	7.9787

航空技術學院學報 第十五卷 第一期(民國一○五年)

Table 3 Comparison of the values of $-\theta'(\chi,0)$ for various values of with

$$N=0,\,m=1/3,\,M=0,\,R_d\!=\!0$$

Table 5 Comparison of the values of $-\phi'(0,0)$	for
various values of N and Le with	
$m = 0 M = 0 R_1 = 0$	

	$-\theta'(\chi,0)$					
χ	Cheng	Yih	Chamkha et	Present		
	[11]	[13]	al. [15]	results		
0.0	0.4272	0.4437	0.4437	0.4437		
0.1	0.3910	0.4044	0.4043	0.4044		
0.2	0.3699	0.3769	0.3769	0.3769		
0.3	0.3667	0.3643	0.3643	0.3643		
0.4	0.3817	0.3686	0.3687	0.3687		
0.5	0.4131	0.3900	0.3901	0.3900		
0.6	0.4574	0.4261	0.4261	0.4261		
0.7	0.5113	0.4731	0.4732	0.4731		
0.8	0.5721	0.5278	0.5280	0.5278		
0.9	0.6378	0.5878	0.5879	0.5878		
1.0	0.7071	0.6515	0.6516	0.6515		
1.0	.0 0.7071 0.6515 0.65	0.6516	(0.6515)			

Result in parenthesis is analytical solution by Eq. (35)

Table 4 Comparison of the values of $-\theta'(0,0)$ for various values of N and Le with

	$m = 0, M = 0, R_d = 0$							
		$-\theta'(0,0)$						
		Bejan						
N	Le	and	Cheng	Yih	Present			
		Khair	[19]	[20]	results			
		[18]						
4	1	0.992	1.070	0.9923	0.9922			
	10	0.681	0.720	0.6810	0.6810			
	100	0.521	0.553	0.5209	0.5207			
1	1	0.628	0.667	0.6276	0.6275			
	10	0.521	0.557	0.5215	0.5214			
	100	0.470	0.504	0.4702	0.4700			

		$-\phi'(0,0)$					
		Bejan					
N	Le	and	Cheng	V:b [20]	Present		
		Khair	[19]	Yih [20]	results		
		[18]					
4	1	0.992	1.070	0.9923	0.9922		
	10	3.290	3.570	3.2897	3.2897		
	100	10.521	11.452	10.5205	10.5203		
1	1	0.628	0.677	0.6276	0.6275		
	10	2.202	2.410	2.2021	2.2019		
	100	7.139	7.876	7.1391	7.1345		

Table 6 Comparison of the values of $-\theta'(\chi,0)$ and $-\phi'(\chi,0)$ for various values of Le with $N=1,\,m=1/2,\,M=0,\,R_d=0$

		-θ' ($(\chi,0)$	-φ'((χ,0)
Le	χ	Yih	Present	Yih	Present
		[6]	results	[6]	results
0.01	0.0	0.7139	0.7139	0.0470	0.0470
	0.5	0.4851	0.4851	0.0411	0.0411
	1.0	0.6910	0.6910	0.0691	0.0691
1	0.0	0.6276	0.6275	0.6276	0.6275
	0.5	0.4559	0.4559	0.4559	0.4559
	1.0	0.6910	0.6910	0.6910	0.6910
100	0.0	0.4700	0.4700	7.1390	1.1389
	0.5	0.4108	0.4108	4.8510	4.8477
	1.0	0.6910	0.6910	6.9099	6.9097

Table 7 Comparison of the values of $Nu_x/(Pe_x^{\frac{1}{2}}+Ra_x^{\frac{1}{2}}) \ \ \text{for various values of } R_d \ \text{and } H$ with $N=0,\,M=0,\,\chi=0$

	$Nu_{x}/(Pe_{x}^{1/2}+Ra_{x}^{1/2})$					
D	H =	: 1.1	H = 3			
R_d	Yih	Present	Yih	Present		
	[21]	results	[21]	results		
0	0.4437	0.4437	0.4437	0.4437		
1		0.7220		2.0852		
5		1.3487		4.5758		
10	1.8549	1.8550		6.4553		

Table 8 Comparison of the values of $Nu_x/(Pe_x^{\frac{1}{2}} + Ra_x^{\frac{1}{2}})$ for various values of χ , R_d and m with N=0, M=0, H=1.0001

	D	Nı	$u_x / (Pe_x^{1/2} + Ra)$	½)
χ	R_d	m = 0	m = 1/3	m = 1
0.0	0	0.4437	0.4437	0.4437
0.0	U	(0.4437)	(0.4437)	(0.4437)
	1	0.6779	0.6779	0.6779
	5	1.2288	1.2288	1.2288
	10	1.6802	1.6802	1.6802
0.5	0	0.3603	0.3900	0.4261
0.3	U	(0.3603)	(0.3900)	(0.4227)
	1	0.5504	0.5958	0.6422
	5	0.9977	1.0799	1.1632
	10	1.3642	1.4766	1.6104
1.0	0	0.5642 (0.5642)	0.6515 (0.6515)	0.7979 (0.7979)
	1	0.8619	0.9952	1.2189
	5	1.5623	1.8038	2.2094
	10	2.1361	2.4666	3.0210

Results in parentheses are those of Yih [13]

The following numerical results are graphically and tabularly presented for the buoyancy ratio N ranging from 1 to 4, the Lewis

number Le ranging from 1 to 10, the wedge angle parameter m ranging from 0 to 1, the magnetic parameter M ranging from 0 to 2, the mixed convection parameter χ ranging from 0 to 1, the radiation-conduction parameter R_d ranging from 0 to 10, and the surface temperature parameter H ranging from 1.1 to 3.

Figures 2 and 3 show the dimensionless temperature and concentration profiles for two values of the wedge angle parameter m (m = 0, 1)and the magnetic parameter M (M = 1, 2) with R_d = 5, H = 3, N = 2, Le = 3, χ = 0.5, respectively. From these two figures, it is found that not only the dimensionless temperature profile but also the dimensionless concentration profile decreases monotonically from the surface to the ambient. On the one hand, for the fixed value of M, both the dimensionless wall temperature gradient $-\theta'(\chi,0)$ and the dimensionless wall concentration gradient $[-\phi'(\chi,0)]$ increase as the wedge angle parameter m is enhanced. That is owing to the fact that an increase in the wedge angle parameter m results in an increase in the flow velocity; thus decreasing the dimensionless temperature profile $\theta(\gamma,\eta)$ and the dimensionless concentration profile $\phi(\chi,\eta)$, and increasing the dimensionless wall temperature gradient and the dimensionless wall concentration gradient.

On the other hand, for the fixed value of m, the dimensionless temperature and concentration profiles increase with increasing the magnetic parameter M. The application of a magnetic field results in slowing the fluid flow velocity. This fact can also be demonstrated from equation (16). Therefore, both the dimensionless wall temperature gradient and the dimensionless wall concentration gradient reduce as M increases.

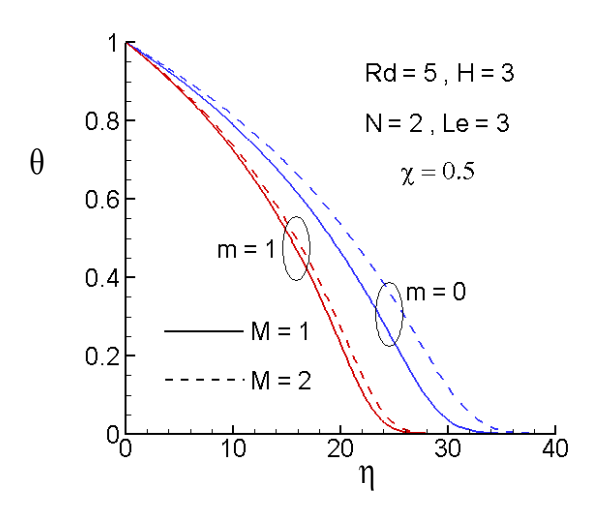


Fig. 2. Dimensionless temperature profile for two values of m and M

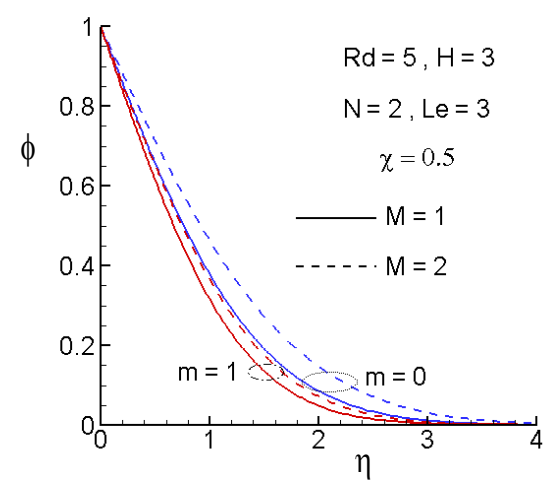


Fig. 3. Dimensionless concentration profile for two values of m and M

Tables 9 and 10 show the values of $Nu_x/(Pe_x^{\frac{1}{2}}+Ra_x^{\frac{1}{2}})$ and $Sh_x/(Pe_x^{\frac{1}{2}}+Ra_x^{\frac{1}{2}})$ for the various values of χ , m and M with $R_d=5$, H=3, N=2, Le=3, respectively. On the one hand, for the fixed value of χ and M, an increase in the wedge angle parameter m tends to increase the local Nusselt number as well as the local Sherwood number. This is due to the fact when the wedge

angle parameter m increases the dimensionless wall $[-\theta'(\chi,0)]$ temperature gradient and dimensionless wall concentration gradient $[-\phi'(\chi,0)]$, as shown in Figs. 2 and 3. With the help of equations (30)-(31), the greater the dimensionless wall temperature gradient and the dimensionless wall concentration gradient, the larger the local Nusselt number and the local Sherwood number. The phenomenon is more pronounced in forced-convection dominated flows $(\chi \text{ approaches to } 1.0)$ than in free-convection dominated flows (χ approaches to 0.0).

On the other hand, an increase in the magnetic parameter M decreases both the local Nusselt number and the local Sherwood number, for the given value of χ and m. That is because increasing the magnetic parameter M tends to decrease the dimensionless wall temperature and concentration gradients, as illustrated in Figs. 2 and 3. This behavior is more evident in the free-convection dominated flow (χ approaches to 0.0) than in forced-convection dominated flows (χ approaches to 1.0).

Table 9 The values of $Nu_x/(Pe_x^{\frac{1}{2}} + Ra_x^{\frac{1}{2}})$ for the various values of χ , m and M with

	$\operatorname{Nu}_{x}/(\operatorname{Pe}_{x}^{\frac{1}{2}}+\operatorname{Ra}_{x}^{\frac{1}{2}})$					
χ	m =	: 0	m = 1			
	M = 1	M = 2	M = 1	M = 2		
0.0	3.4156	2.1606	3.4156	2.1606		
0.2	2.9376	2.0350	3.0389	2.1843		
0.5	3.1624	2.8626	3.9131	3.7747		
0.8	4.2806	4.2459	5.9730	5.9724		
1.0	5.2780	5.2780	7.4642	7.4642		

Table 10 The values of $\operatorname{Sh}_x/(\operatorname{Pe}_x^{\frac{1}{2}}+\operatorname{Ra}_x^{\frac{1}{2}})$ for the various values of χ , m and M with

\mathbf{R}_{A}	= 5.	H =	: 3.	N=	= 2.	Le =	3
- C(1	,	11 -	,	T 4 -	,		

	$Sh_{x}/(Pe_{x}^{\frac{1}{2}}+Ra_{x}^{\frac{1}{2}})$					
χ	m =	0	m = 1			
	M = 1	M = 2	M = 1	M = 2		
0.0	1.0360	0.6552	1.0360	0.6552		
0.2	0.8517	0.5596	0.8613	0.5750		
0.5	0.7126	0.5886	0.8062	0.7224		
0.8	0.8089	0.7927	1.1068	1.1058		
1.0	0.9772	0.9772	1.3819	1.3819		

It is also found that for the same value of M, the values of $Nu_x/(Pe_x^{\frac{1}{2}}+Ra_x^{\frac{1}{2}})$ and $Sh_x/(Pe_x^{\frac{1}{2}}+Ra_x^{\frac{1}{2}})$ at the mixed convection parameter $\chi=0.0$ (pure free convection) in Tables 9 and 10 are independent of the variation of the wedge angle parameter m. These results are also seen from the equations (16)-(18). For the case of $\chi=0.0$, the wedge angle parameter m is disappeared, equations (16)-(18) are reduced to be as follows:

$$(1+M^2) f' = \theta + N \phi, \qquad (36)$$

$$\theta'' + \frac{1}{2}f\theta' + \frac{4R_d}{3} \left\{ \theta' [(H-1)\theta + 1]^3 \right\}' = 0, \quad (37)$$

$$\frac{1}{Le}\phi'' + \frac{1}{2}f\phi' = 0.$$
 (38)

Besides, for the fixed m, the values of $Nu_x/(Pe_x^{\frac{1}{2}}+Ra_x^{\frac{1}{2}})$ and $Sh_x/(Pe_x^{\frac{1}{2}}+Ra_x^{\frac{1}{2}})$ at $\chi=1.0$ (pure forced convection) in Tables 9 and 10 are independent of the variation of the magnetic parameter M. This is because for the case of $\chi=1.0$, the effect of the magnetic parameter M is fading away, equations (16)-(18) are changed to be as follows:

$$f' = 1,$$
 (39)

$$\theta'' + \frac{1+m}{2}f\theta' + \frac{4R_d}{3} \left\{ \theta' [(H-1)\theta + 1]^3 \right\}' = 0, (40)$$

$$\frac{1}{\text{Le}}\phi'' + \frac{1+m}{2}f\phi' = 0. \tag{41}$$

Moreover, as χ varies from 0 to 1, both the local Nusselt number and the local Sherwood number decrease initially, reach a minimum at an intermediate value of χ and then increase gradually, as shown in Tables 9 and 10. The phenomena of minimum are also found in Yih [13-14] and Chamkha et al. [15]. This minimum does not imply a corresponding minimum value in the local Nusselt number and local Sherwood number. This is due to the nature of $Nu_x/(Pe_x^{1/2} + Ra_x^{1/2})$ and $Sh_{\nu}/(Pe_{\nu}^{\frac{1}{2}} + Ra_{\nu}^{\frac{1}{2}})$ vs. γ . For example, let us consider the present numerical results of $Nu_{_X} / (Pe_{_X}^{1/2} + Ra_{_X}^{1/2}) \ \ with \ m=0, \ M=1, \ R_d=5, \ H$ = 3, N = 2, Le = 3 and χ = 0.5 in Table 9. If the local Peclet number is taken as $Pe_x = 100$, the corresponding modified local Rayleigh number can be found to be $Ra_x = 100$ from equation (15.1). the present numerical results $Nu_{_{X}}\,/(Pe_{_{X}}^{1/2}+Ra_{_{X}}^{1/2})\text{, the value of }Nu_{_{X}}$ for mixed convection ($Pe_x = 100$, $Ra_x = 100$) is 63.248. While, for pure free convection ($\chi = 0.0$) and pure forced convection ($\chi = 1.0$) the Nu_x values are found to be 34.156 and 52.78, respectively. Therefore, it is obvious that the present result of Nux for mixed convection is higher than that for pure free convection and pure forced convection.

Figures 4 and 5 illustrate the dimensionless temperature profile and the dimensionless concentration profile for two values of the radiation-conduction parameter R_d ($R_d=1,\,10$) and the surface temperature parameter H (H = 1.1, 2) with m = 1/3, M = 0, N = 1, Le = 1, $\chi=0.5$, respectively. When the radiation-conduction

parameter R_d and the surface temperature parameter increase, the dimensionless temperature profile $\theta(\chi,\eta)$ becomes large, but the dimensionless wall temperature gradient $[-\theta'(\chi,0)]$ becomes small, as shown in Fig. 4. This is on an account the fact as the value of R_{d} or H increases, the radiation absorption in the boundary layer increases, causing the dimensionless temperature profile become large.

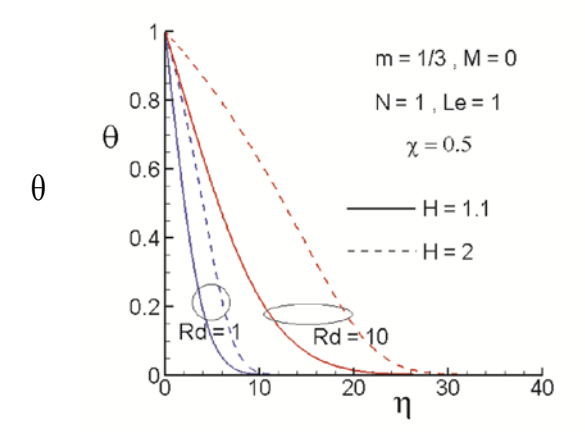


Fig. 4. Dimensionless temperature profile for two values of R_d and H

However, the dimensionless wall concentration gradient $\left[-\phi'(\chi,0)\right]$ enhances a little with increasing the radiation-conduction parameter R_d and the surface temperature parameter H, as displayed in Fig. 5.

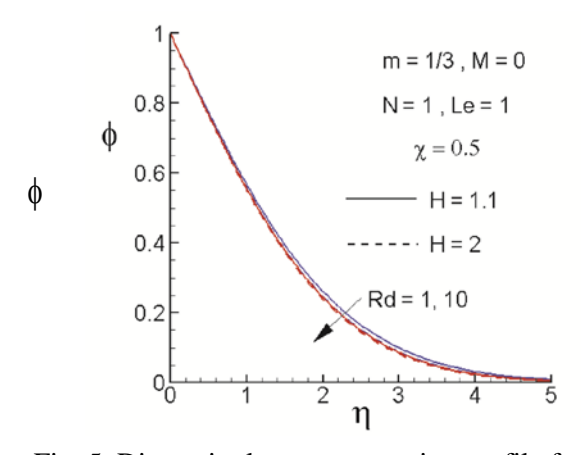


Fig. 5. Dimensionless concentration profile for two values of R_d and H

Tables 11 and 12 illustrate the values of $Nu_x / (Pe_x^{\frac{1}{2}} + Ra_x^{\frac{1}{2}})$ and $Sh_x / (Pe_x^{\frac{1}{2}} + Ra_x^{\frac{1}{2}})$ for the various values of χ , R_d and H with m = 1/3, M = 0, N = 1, Le = 1, respectively. For the fixed value of χ , both the local Nusselt number and the local Sherwood number increase radiation-conduction parameter R_d and the surface temperature parameter H increase. In the pure mixed convection heat transfer, the local Nusselt number is only proportional to the dimensionless wall temperature gradient $[-\theta'(\chi,0)]$. For the case of large R_d and H (radiation effect becomes pronounced), although the value of $\left[-\theta'(\chi,0)\right]$ is low, as shown in Fig. 4, the local Nusselt number is still large. This is because the local Nusselt number is found to be more sensitive to R_d and H than $|-\theta'(\chi,0)|$, as revealed in Eq. (30).

Moreover, the local Nusselt number is significantly increased for large values of the radiation-conduction parameter R_d and the surface temperature parameter H; i.e., the radiation effect becomes pronounced. However, increasing the radiation-conduction parameter R_d and the surface temperature parameter H has the tendency to enhance slightly the local Sherwood number, as compared in Tables 11 and 12.

In addition, the present values of $Sh_x/(Pe_x^{\frac{1}{2}}+Ra_x^{\frac{1}{2}})$ at $\chi=1.0$ (pure forced convection) in Table 12 are independent of the variation of the radiation-conduction parameter R_d and the surface temperature parameter H. This result could be revealed with the aid of equations (39) and (41).

Table 11 The values of $Nu_x/(Pe_x^{\frac{1}{2}}+Ra_x^{\frac{1}{2}})$ for the various values of χ , R_d and H with

$$m = 1/3$$
, $M = 0$, $N = 1$, $Le = 1$

	$\operatorname{Nu}_{x}/(\operatorname{Pe}_{x}^{\frac{1}{2}}+\operatorname{Ra}_{x}^{\frac{1}{2}})$			
χ	$R_d = 1$		$R_d = 10$	
	H = 1.1	H = 2	H = 1.1	H = 2
0.0	0.9414	1.5069	2.1064	4.0212
0.2	0.7821	1.2551	1.7701	3.3739
0.5	0.7024	1.1483	1.7051	3.2450
0.8	0.8607	1.4248	2.1918	4.1881
1.0	1.0518	1.7432	2.6912	5.1449

Table 12 The values of $\operatorname{Sh}_x/(\operatorname{Pe}_x^{1/2}+\operatorname{Ra}_x^{1/2})$ for the various values of χ , R_d and H with

$$m = 1/3$$
, $M = 0$, $N = 1$, $Le = 1$

	$\operatorname{Sh}_{x}/(\operatorname{Pe}_{x}^{1/2}+\operatorname{Ra}_{x}^{1/2})$			
χ	$R_d = 1$		$R_d = 10$	
	H = 1.1	H = 2	H = 1.1	H = 2
0.0	0.6678	0.6993	0.7040	0.7151
0.2	0.5483	0.5729	0.5766	0.5849
0.5	0.4595	0.4710	0.4726	0.4770
0.8	0.5359	0.5374	0.5376	0.5383
1.0	0.6515	0.6515	0.6515	0.6515
	(0.6515)	(0.6515)	(0.6515)	(0.6515)

Results in parentheses are analytical solution by Eq. (35)

Figures 6 and 7 display the dimensionless temperature and concentration profiles for two values of the buoyancy ratio N (N = 1, 4) and the Lewis number Le (Le = 1, 10) with R_d = 1, H = 1.5, m = 1/2, M = 1, χ = 0.5, respectively. For a fixed value of Le, increasing the buoyancy ratio N increases the buoyancy force, accelerating the flow velocity, thus enhancing not only the dimensionless wall temperature gradient $\left[-\theta'(\chi,0)\right]$ but also the

dimensionless wall concentration gradient $[-\phi'(\chi,0)]$, as illustrated in Figs. 6 and 7.

For case of the fixed N, when the Lewis number Le increases from 1 to 10, the dimensionless wall temperature gradient decreases but the thermal boundary layer thickness δ_T becomes thick, as shown in Fig. 6. Whereas, the dimensionless wall concentration gradient increases yet the concentration boundary layer thickness δ_C becomes thin as the Lewis number is increased, as shown in Fig. 7.

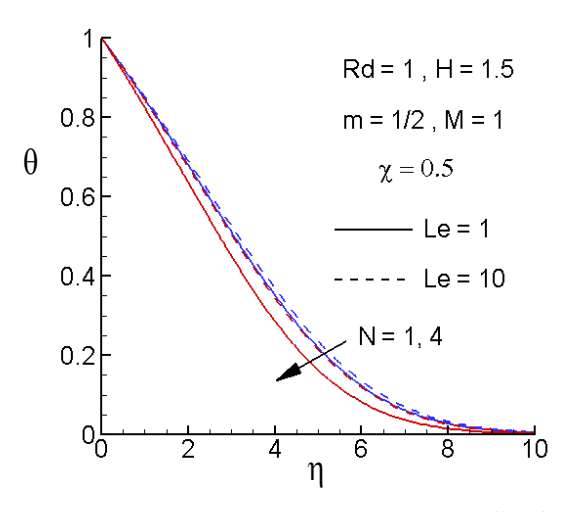


Fig. 6. Dimensionless temperature profile for two values of N and Le

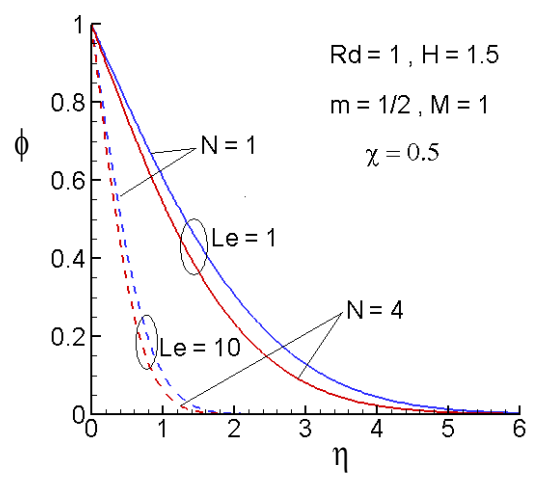


Fig. 7. Dimensionless concentration profile for two values of N and Le

Tables 13 and 14 depict the values of $Nu_x/(Pe_x^{\frac{1}{2}} + Ra_x^{\frac{1}{2}})$ and $Sh_x/(Pe_x^{\frac{1}{2}} + Ra_x^{\frac{1}{2}})$ for the various values of χ , N and Le with $R_d = 1$, H = 1.5, m = 1/2, M = 1, respectively. Increasing the buoyancy ratio N tends to increase the local Nusselt number as well as the local Sherwood number. This is due to the fact when the buoyancy ratio N enhances both the dimensionless wall $[-\theta'(\chi,0)]$ temperature gradient and the dimensionless wall concentration gradient $[-\phi'(\chi,0)]$, as shown in Figs. 6 and 7. For the fixed R_d and H, with the aid of equations (30)-(31), the larger the dimensionless wall temperature gradient and the dimensionless wall concentration gradient, the greater the local Nusselt number and the local Sherwood number.

In Table 13 (Table 14), we can find that the local Nusselt (Sherwood) number decreases (increases) as the Lewis number Le is increased, for the fixed N and χ . This is due to the fact that a larger Lewis number Le is associated with a thicker thermal boundary layer thickness δ_T but a thinner concentration boundary layer thickness δ_C , as illustrated in Figs. 6 and 7. The thicker the thermal boundary layer thickness, the smaller the local Nusselt number. The thinner the concentration boundary layer thickness, the greater the local Sherwood number.

Furthermore, the present values of $Nu_x/(Pe_x^{\frac{1}{2}}+Ra_x^{\frac{1}{2}})$ at $\chi=1.0$ (pure forced convection) in Table 13 are independent of the variations of the buoyancy ratio N and the Lewis number Le. This result could be revealed with the aid of equations (39)-(40). For the fixed Le, the present values of $Sh_x/(Pe_x^{\frac{1}{2}}+Ra_x^{\frac{1}{2}})$ at $\chi=1.0$ (pure forced convection) in Table 14 are independent of the variation of the buoyancy ratio

N. This result could be expressed with the help of equations (39) and (41).

Table 13 The values of $\operatorname{Nu}_{x}/(\operatorname{Pe}_{x}^{\frac{1}{2}}+\operatorname{Ra}_{x}^{\frac{1}{2}})$ for the various values of χ , N and Le with

$$R_d = 1, H = 1.5, m = 1/2, M = 1$$

	$Nu_{x}/(Pe_{x}^{\frac{1}{2}}+Ra_{x}^{\frac{1}{2}})$			
χ	N = 1		N = 4	
	Le = 1	Le = 10	Le = 1	Le = 10
0.0	0.8252	0.7177	1.1718	0.8308
0.2	0.7141	0.6349	0.9813	0.7248
0.5	0.8016	0.7770	0.9110	0.8184
0.8	1.1318	1.1294	1.1430	1.1337
1.0	1.4028	1.4028	1.4028	1.4028

Table 14 The values of $\operatorname{Sh}_{x}/(\operatorname{Pe}_{x}^{\frac{1}{2}}+\operatorname{Ra}_{x}^{\frac{1}{2}})$ for the various values of χ , N and Le with

$$R_d = 1$$
, $H = 1.5$, $m = 1/2$, $M = 1$

	$Sh_{x}/(Pe_{x}^{\frac{1}{2}}+Ra_{x}^{\frac{1}{2}})$			
χ	N = 1		N = 4	
	Le = 1	Le = 10	Le = 1	Le = 10
0.0	0.4846	1.5920	0.7295	2.3495
0.2	0.4079	1.3363	0.5974	1.9227
0.5	0.4112	1.3175	0.4902	1.5665
0.8	0.5590	1.7694	0.5671	1.7952
1.0	0.6910	2.1849	0.6910	2.1849
	(0.6910)	(2.1851)	(0.6910)	(2.1851)

Results in parentheses are analytical solution by Eq. (35)

5. Conclusions

A laminar boundary layer analysis is presented to study the thermal radiation with Rosseland diffusion approximation and the magnetic effects on the coupled heat and mass transfer by combined natural and forced convection flow from a wedge with uniform wall temperature and uniform wall concentration (UWT/UWC) in porous media saturated with an optically dense, electrically conducting viscous fluid in the presence of a transverse magnetic field. The resulting governing equations are dimensionless and transformed into a non-similar form and then solved using an implicit, finite-difference method (Keller box method: KBM). A comparison is made with the available results in the literature, and our results are in very good agreement with the known results. Numerical solutions are obtained for different values of the buoyancy ratio N, the Lewis number Le, the wedge angle parameter m, the magnetic parameter M, the mixed convection parameter the χ, radiation-conduction parameter R_d, and the surface temperature parameter H in graphical and tabular forms. The entire regime of the mixed convection is included, when χ varies from 0 (pure free convection) to 1 (pure forced convection). The decay of the dimensionless temperature and concentration profiles has been observed in all cases.

The significant features of the results are summary as follows:

- 1. Not only the local Nusselt number but also the local Sherwood number decreases initially, reaches a minimum in the intermediate value of χ , and then increases gradually.
- 2. An increase in the wedge angle parameter m tends to increase the local Nusselt number as well as the local Sherwood number, whereas an increase in the magnetic parameter M decreases both the local Nusselt number and the local Sherwood number.
- 3. The local Nusselt number is significantly increased for large values of the radiation–conduction parameter $R_{\rm d}$ and the surface

temperature parameter H; i.e., the radiation effect becomes pronounced. However, increasing the radiation—conduction parameter $R_{\rm d}$ and the surface temperature parameter H has the tendency to enhance slightly the local Sherwood number.

4. It is also found that increasing the buoyancy ratio N increases not only the local Nusselt number but also the local Sherwood number. As the Lewis number Le increases, the local Nusselt (Sherwood) number decreases (increases).

Nomenclature

- a_r Rosseland mean extinction coefficient
- B constant
- B_o externally imposed magnetic field
- C concentration
- C_P specific heat at constant pressure
- D_M mass diffusivity
- f dimensionless stream function
- g gravitational acceleration
- H surface temperature parameter
- h_x local convective heat transfer coefficient
- $h_{\text{m.x}}$ local convective mass transfer coefficient
- K permeability of the porous medium
- k equivalent thermal conductivity
- Le Lewis number
- M magnetic parameter
- m wedge angle parameter
- mw local mass flux
- N buoyancy ratio
- Nu_x local Nusselt number
- p pressure of fluid
- Pe_x local Peclet number
- q_{cond} conductive heat flux
- q_r radiative heat flux
- qw local heat flux
- R_d radiation-conduction parameter

航空技術學院學報 第十五卷 第一期(民國一○五年)

- Ra_x modified local Rayleigh number
- Sh_x local Sherwood number
- T temperature
- U_{∞} velocity of the potential flow outside the boundary layer
- u Darcy velocity in the x-direction
- v Darcy velocity in the y-direction
- x streamwise coordinate
- y transverse coordinate

Greek symbols

- α equivalent thermal diffusivity
- $\beta_{\rm C}$ coefficient of concentration expansion
- β_T coefficient of thermal expansion
- γ half angle of wedge
- δ_C concentration boundary layer thickness
- δ_T thermal boundary layer thickness
- η pseudo-similarity variable
- θ dimensionless temperature
- μ viscosity of fluid
- ρ density of fluid
- σ electrical conductivity of fluid
- σ_0 Stefan-Boltzmann constant
- σ_s scattering coefficient
- φ dimensionless concentration
- χ mixed convection parameter
- w stream function

Subscripts

- w condition at the wall
- ∞ condition at infinity

References

- Nield, D. A., and Bejan, A., Convection in Porous Media, 4th Edition, New York, Springer-Verlag (2013).
- 2. Cheng, P., "Combined free and forced

- convection flow about inclined surfaces in porous media," Int. J. Heat Mass Transfer, Vol. 20, pp. 807-814 (1977).
- Lai, F. C., and Kulacki, F. A., "The influence of lateral mass flux on mixed convection over inclined surfaces in saturated porous media," J. Heat Transfer, Vol. 112, pp. 515-518 (1990).
- 4. Vargas, J. V. C., Laursen, T. A., and Bejan, A., "Nonsimilar solutions for mixed convection on a wedge embedded in a porous medium," Int. J. Heat Fluid Flow, Vol. 16, pp. 211-216 (1995).
- 5. Kumari, M., and Gorla, R. S. R., "Combined convection along a non-isothermal wedge in a porous medium," Heat Mass Transfer, Vol. 32, pp. 393-398 (1997).
- 6. Yih, K. A., "Coupled heat and mass transfer in mixed convection over a wedge with variable wall temperature and concentration in porous media: the entire regime," Int. Commun. Heat Mass Transfer, Vol. 25, pp. 1145-1158 (1998).
- Yih, K. A., "Uniform transpiration effect on coupled heat and mass transfer in mixed convection about inclined surfaces in porous media: the entire regime," Acta Mech., Vol. 132, pp. 229-240 (1999).
- 8. Cheng, C. Y., "Soret and Dufour effects on mixed convection heat and mass transfer from a vertical wedge in a porous medium with constant wall temperature and concentration," Trans. Porous Media, Vol. 94, pp. 123-132 (2012).
- Chamkha, A. J., and Khaled, A. R. A., "Nonsimilar hydromagnetic simultaneous heat and mass transfer by mixed convection from a vertical plate embedded in a uniform porous medium," Num. Heat Transfer, Vol. 36, pp. 327-344 (1999).
- 10. Cheng, C. Y., "An integral approach for

- hydromagnetic natural convection heat and mass transfer from vertical surfaces with power-law variation in wall temperature and concentration in porous media," Int. Commun. Heat Mass Transfer, Vol. 32, pp. 204-213 (2005).
- Cheng, C. Y., "Effect of a magnetic field on mixed convection heat and mass transfer from a vertical wedge in a porous medium by an integral approach," J. Southern Taiwan University, Vol. 40, pp. 27-38 (2015).
- 12. Hossain, M. A., and Takhar, H. S., "Radiation effect on mixed convection along a vertical plate with uniform surface temperature," Heat Mass Transfer, Vol. 31, pp. 243-248 (1996).
- 13. Yih, K. A., "Radiation effect on mixed convection over an isothermal wedge in porous media: the entire regime," Heat Transfer Engrg., Vol. 22, pp. 26-32 (2001).
- 14. Yih, K. A, "Radiation and blowing/suction effects on mixed convection over an isothermal vertical cylinder in porous media: the entire regime," J. Air Force Insti. Tech., Vol. 9, pp. 277-286 (2010).
- Chamkha, A. J., Abbasbandy, S., Rashad, A. M., and Vajravelu, K., "Radiation effects on mixed convection over a wedge embedded in a porous medium filled with a nanofluid," Trans. Porous Media, Vol. 91, pp. 261-279 (2012).
- Hong, J. T., Yamada, Y., and Tien, C. L., "The effects of non-Darcian and non-uniform porosity on vertical plate- natural convection in porous media," J. Heat Transfer, Vol. 109, pp. 356-362 (1987).
- 17. Cebeci, T., and Bradshaw, P., Physical and Computational Aspects of Convective Heat

- Transfer, New York, Springer-Verlag (1984).
- Bejan, A., and Khair, K. R., "Heat and mass transfer by natural convection in a porous medium," Int. J. Heat Mass Transfer, Vol. 28, pp. 909-918 (1985).
- 19. Cheng, C. Y., "Effect of magnetic field on heat and mass transfer by natural convection from vertical surfaces in porous media- an integral approach," Int. Commun. Heat Mass Transfer, Vol. 26, pp. 935-943 (1999).
- Yih, K. A., "Coupled heat and mass transfer by free convection over a truncated cone in porous media: VWT/VWC or VHF/VMF," Acta Mech., Vol. 137, pp. 83-97 (1999).
- 21. Yih, K. A, "Effect of radiation on natural convection over an isothermal vertical permeable flat plate in porous media," J. Air Force Insti. Tech., Vol. 7, pp. 131-138 (2008).

航空技術學院學報 第十五卷 第一期(民國一○五年)